Magnetic extended x-ray absorption fine structure at the $L_{3,2}$ edges of 3d elements

1998 J. Phys.: Condens. Matter 10 1917

(http://iopscience.iop.org/0953-8984/10/8/023)

J. Phys.: Condens. Matter **10** (1998) 1917–1930. Printed in the UK PII: S0953-8984(98)86456-4

Magnetic extended x-ray absorption fine structure at the $L_{3,2}$ edges of 3d elements

L Lemke†, H Wende†, P Srivastava†‖, R Chauvistré†, N Haack†, K Baberschke†, J Hunter-Dunn‡, D Arvanitis‡, N Mårtensson‡, A Ankudinov§ and J J Rehr§

† Institut für Experimentalphysik, Freie Universität Berlin, Arnimallee 14, D-14195, Berlin-Dahlem, Germany

‡ Department of Physics, Uppsala University, Box 530, S-75121 Uppsala, Sweden

§ Department of Physics, University of Washington, Seattle, WA 98175, USA

Received 31 July 1997, in final form 12 December 1997

Abstract. We report normal and magnetic extended x-ray absorption fine-structure (EXAFS) measurements made on 30 ML Fe films on Cu(001) substrates at the $L_{3,2}$ edges. The magnetic EXAFS at the L edges of 3d metals is particularly important as it can be used to probe the magnetism of the d states. Magnetic EXAFS oscillations were detected up to 500 eV above the edge, corresponding to 11.5 Å^{-1} in k-space. Over such a large range, we were able to see long-wavelength wiggles and separate them from Fe nearest-neighbour backscattering and the fast oscillations that had been previously seen. It is shown that without using any deconvolution procedure, a meaningful analysis can be performed despite the interference of the L_3 and L_2 edges. The experimental data were compared with the results of multiple-scattering calculations, and this enabled us to assign all of the features in both the normal and the magnetic EXAFS Fourier transforms to various single- and multiple-scattering paths. Also, there was found to be less temperature-dependent damping for magnetic EXAFS as than for the normal EXAFS between 75 K and 300 K.

1. Introduction

The extended x-ray absorption fine-structure (EXAFS) technique is now well established as a chemically selective spectroscopic method not only for local atomic structure determination but also for studying the dynamic behaviour of bonds [1]. This is also the case for the EXAFS formalism. The phase $\phi(T, k)$ and amplitude $A(T, k)$ of a single-shell EXAFS signal can be represented as a sine function:

$$k\chi(T, k) = A(T, k) \sin \phi(T, k). \tag{1}$$

The amplitude $A(T, k)$ and the phase $\phi(T, k)$ are determined by the bond length $R(T)$ between an absorbing and a backscattering atom, the effective coordination number N^* of a given neighbouring shell and the local electronic configuration of the absorber–backscatterer pair. The disorder is described by the non-zero second and third pair distribution function moments, $\sigma^2(T)$ and $c_3(T)$, and the mean square and cubic relative displacements (MSRD and MCRD). The MSRD is also known as the EXAFS Debye–Waller factor.

‖ Author to whom any correspondence should be addressed; e-mail: babgroup@physik.fu-berlin.de; fax: +(49) 30 838 3646. Permanent address: Department of Physics, University of Rajasthan, Jaipur-302 004, India.

0953-8984/98/081917+14$19.50

The separation of $k\chi(T,k)$ into amplitude and phase contributions yields

$$A(T,k) = N^* F(k) R(T)^{-2} S_0^2 \exp[-2R(T)/\lambda(k)] \exp[-2k^2\sigma^2(T)] \quad (2)$$

$$\phi(T,k) = 2k[R(T) - \sigma^2(T)[1/R(T) + 2/\lambda]] - (4/3)k^3 c_3(T) + \varphi(k). \quad (3)$$

A complete explanation of the above equations is not needed in the present analysis; however, a detailed explanation of the equations and the symbols is given in [2–4]. Strictly speaking, equation (1) in combination with equations (2) and (3) only holds true for K- and L_1-edge EXAFS. The EXAFS formula for $L_{3,2}$ edges is more complex owing to the fact that the initial p state can go on to exhibit final-state s or d symmetry. However, transitions to the d final state are favoured by a factor of 20 as compared to transitions to s final states and the system under study has a cubic symmetry. Therefore, for all practical purposes the $L_{3,2}$-edge EXAFS can be analysed in the same way as that of the K and L_1 edges (for details, see [1]).

With the availability of circularly polarized synchrotron radiation the total absorption coefficient $\mu(E)$ for normal EXAFS can be defined as

$$\mu(E) = [\mu^+(E) + \mu^-(E)]/2 \quad (4)$$

where μ^+ and μ^- are the spin absorption coefficients for right and left circularly polarized light.

This enables one to add magnetic selectivity to the EXAFS technique. The absorption of left circularly polarized photons is different from that of right circularly polarized photons at the absorption edges. Therefore, the spin-dependent part of the backscattering amplitude leads to there being different EXAFS oscillations in the cases where the photon spin is parallel and where it is antiparallel to the spin of the electrons in the absorber. The difference in the spin-polarized EXAFS, i.e. the magnetic EXAFS (MEXAFS), can be determined by measuring the spin-dependent absorption in the EXAFS energy range. The magnetic absorption coefficient can be written as

$$\mu_M(E) = \mu^+(E) - \mu^-(E). \quad (5)$$

Throughout the text, the modulations in the EXAFS and MEXAFS signals are called χ and χ_M respectively (see equation (6)).

The MEXAFS has opened up a new field of research, allowing the investigation of static and dynamic magnetic phenomena to be carried out from a site-selective point of view [5–17]. The earlier MEXAFS experiments on the 3d transition metal K edges [5, 8, 12–15] and 4f rare-earth L edges [6, 8, 13–15] have shown that by means of this technique it is possible to study the magnetic short-range order and gain insight into the magnetic spin moments of neighbouring atoms. In the case of pure 3d metals (Fe, Co, Ni), it was found that the K-edge MEXAFS oscillations are in phase with the EXAFS oscillations, indicating that this effect is primarily due to the scattering from magnetic nearest neighbours [8, 12, 13, 15]. Furthermore, the absence of the peak corresponding to nearest-neighbour oxygen atoms in the Fourier transforms of the MEXAFS data for garnets ($Eu_3Fe_5O_{12}$ and $Ho_3Fe_5O_{12}$) supports this notion [8, 15]. Also, it demonstrates that one can distinguish between magnetic and non-magnetic neighbours by comparing the EXAFS and MEXAFS Fourier transforms.

The first MEXAFS measurements that were reported were made at the K edge of ferromagnetic iron [5]. However, studies at K edges, which are very common in EXAFS investigations, have some disadvantages if one wishes to investigate MEXAFS, as one probes final p states. This p-state probing, especially in the case of 3d transition metals, produces no information about the d states, which provide the main contribution to

the magnetism, and also results in a lower MEXAFS signal. Consequently, MEXAFS measurements at the $L_{3,2}$ edges of rare-earth elements (Gd, Tb) have been reported [6]. For elements like Gd, the separation between the L_3 and L_2 edges is around 690 eV, allowing one to analyse the two edges separately. This has been shown in the past to be the case for the EXAFS of, for example, the pseudobinary compound $La_{1-x}Gd_xOs_2$ [18], and recently also for a MEXAFS study of Gd metal and $Gd_3Fe_5O_{12}$ [6, 8]. However, the MEXAFS at the L edges of the rare-earth elements probes final d states and not the 4f shell, while the latter carries most of the magnetic information. On the other hand, in the case of 3d transition metals (Fe, Co, Ni), substantial difficulties are expected as regards EXAFS and MEXAFS studies due to the smaller spin–orbit splitting (13.1 eV for Fe, 15.2 eV for Co and 17.3 eV for Ni) between the L_3 and L_2 edges. This leads to an additive overlap of the two edges, which, in the case of the MEXAFS, may also partly cancel the signal, as the dichroic effects have the same profiles but opposite signs. Therefore, it was necessary to address the problems stated above in order to carry out a meaningful MEXAFS analysis at the L edges of transition metals, which, in view of the strong dipole transition to the magnetically interesting 3d states and the larger MEXAFS effect, are the obvious choice for studying.

Recently, the first MEXAFS measurements at the $L_{3,2}$ edges of 3d transition metals were reported [9, 10]. These measurements were carried out on polycrystalline Fe, Co and Ni films (250–300 Å thick) grown on parylene substrates. To separate the MEXAFS oscillations of the individual L_3 and L_2 edges, an iterative Van Cittert deconvolution method was used in energy space. These experiments showed enhancements for the larger distances of 4–5 Å for the spin-dependent scattering of the photoelectron. However, the nearest-neighbour peak reported for the bcc Fe at around 2.49 Å was very broad in the Fourier transforms [10]. This may be due either to the sample being polycrystalline or to the k-range used for the Fourier transformation.

In the present contribution, we report temperature-dependent (75–300 K) EXAFS and MEXAFS measurements on a 30 ML Fe film on a Cu(001) substrate that extend up to 500 eV above the $L_{3,2}$ edges. The experimental data are compared with multiple-scattering (MS) calculations, which allows us to identify all of the main features in the EXAFS and MEXAFS Fourier transforms. Our analysis clearly shows that there is no need to carry out any fitting procedure to deal with the interference of the L_3 and L_2 edges.

The organization of this article is as follows. All of the experimental details and the method of analysing the data are discussed in section 2. Thereafter, the temperature-dependent normal EXAFS and MEXAFS analysis of the Fe film and how it compares with MS calculations are described in sections 3 and 4 respectively. To the best of our knowledge, this is the first L-edge MEXAFS study of a 3d ferromagnet which reports in parallel the ordinary and magnetic EXAFS of the nearest and next-nearest neighbours as well as the multiple-scattering effects.

2. Experimental and data analysis details

Thin Fe films, 30 ML thick, on Cu(001) were chosen as a prototype. The films were grown at room temperature on Cu(001) substrates in ultrahigh-vacuum (UHV) conditions and characterized by means of *in situ* LEED. Fe/Cu(001) is one of the most prominent ultrathin-film systems and its mode of growth is well understood [19]. The chosen thickness and the Cu substrate hold several advantages for our MEXAFS experiment. One would like to have a fairly thick Fe film and a single-crystal-like structure with a minimum of local disorder to enlarge the signal. In section 3, it is shown that we do indeed have a bcc structure.

On the other hand, one would also like to prepare thinner films in which the L edges of Cu around 932 and 952 eV shine through in the XAFS spectrum. With these samples, we did test that our normalization and separation of the MEXAFS are exactly correct. For the thin films, the Cu and Fe EXAFS will be superimposed, whereas for the MEXAFS (see section 4) no signal $\mu_M(E)$ is expected for Cu. The L-edge spectra were recorded in a quasi-total-electron-yield mode at normal (90°) and grazing (20°) x-ray incidences at 300 K and 75 K using circularly polarized light at the SX 700 monochromator beamlines at BESSY synchrotron facility in Berlin. The other experimental details are described elsewhere [20]. For this thickness range, the easy axis of the magnetization was found to be in the plane and therefore no MEXAFS oscillations were observed in the spectra measured at normal x-ray incidence. As the aim of this study is to compare normal and magnetic EXAFS, we discuss only the spectra recorded at grazing (20°) x-ray incidence. However, we wish to make it clear that spectra recorded at normal x-ray incidence were also analysed for normal EXAFS.

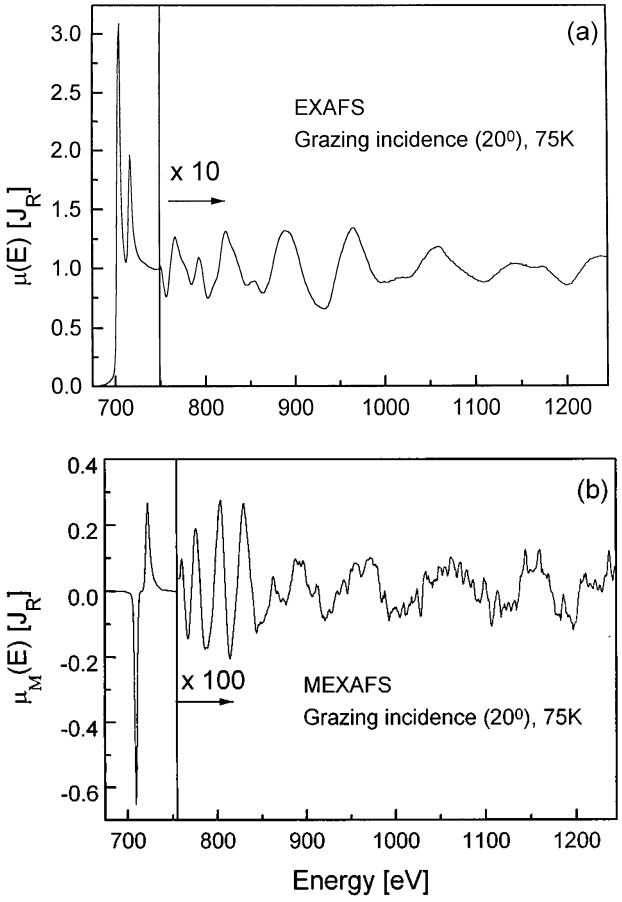

Figure 1. The $L_{3,2}$ (a) EXAFS and (b) MEXAFS spectra for a 30 ML Fe film on Cu(001). The spectra were recorded at grazing x-ray incidence (20°) at 75 K. The region containing the extended fine structure has been expanded as indicated in each panel. The total ($\mu(E)$) and magnetic ($\mu_M(E)$) absorption coefficients are shown in units of the edge jump (J_R). As a result the relative scales for $\mu(E)$ and $\mu_M(E)$ are not arbitrary.

In the analysis of the EXAFS in the soft-x-ray regime it is a standard technique to subtract a spline (background) from the rough $\mu(E)$ data, for both bulk [3] and surface experiments [4]. This is also necessary for the normal $L_{3,2}$ EXAFS, and is not a problem as the signals are large (see section 3). $E_0(k = 0)$ for the photoelectron kinetic energy was chosen to lie at the inflection point of the L_3 edge (707 eV). For the simulation, E_0 for the L_2 edge was chosen to be 720 eV. Taking the difference of the right and left polarizations for the MEXAFS as defined in equation (5), one may think at first glance that the background (transmission function etc) is automatically subtracted and therefore that $\mu_M(E)$ is easier to determine than $\mu(E)$. However, it was found in the present experiments that this did not work satisfactorily because of the small changes in the background as a function of time irrespective of the detection mode and sequence used. The best method was found to be that of taking a ratio, and deriving χ_M from $\mu_M \approx [(\mu^+/\mu^-) - 1]\mu_0$ instead of the difference $\mu_M \equiv \mu^+ - \mu^-$. It can easily be shown that these two approaches are equivalent, provided that $\mu^+ + \mu^- \gg \mu^+ - \mu^-$; here, $(\mu^+ - \mu^-)/(\mu^+ + \mu^-) < 10^{-2}$. On making some approximations, it can be shown that $1 + \chi_M \approx \mu^+/\mu^-$. Both EXAFS and MEXAFS oscillations were detected up to approximately 1300 eV, which corresponds in k-space to 11.5 Å^{-1}. Figures 1(a) and 1(b) show Fe $L_{3,2}$ absorption and the dichroism spectra respectively, after subtraction of a cubic spline and normalization of the combined edge jump to one. In both cases, the energy regions in which the EXAFS and MEXAFS oscillations lie are vertically expanded. Both spectra are normalized to the edge jump, i.e. the number of Fe atoms. This is the same procedure as is followed in EXAFS analysis. In both spectra, one observes oscillations over the whole energy range, with an amplitude of the order of 9% for ordinary EXAFS and 0.3% for the magnetic EXAFS. This is one important result of the present experiments: the MEXAFS at L edges of Fe, Co is fairly large—less than an order of magnitude smaller than the normal EXAFS. It was most important to record the spectra up to ≈1300 eV. This is necessary to identify in the EXAFS and MEXAFS the backscattering by the nearest neighbours. In particular, for the spin-dependent backscattering the amplitude $A(T, k)$ and phase $\phi(T, k)$ need to be compared with theoretical calculations. Figure 1(b) shows not only the 'fast' oscillations in the first 150 eV above the L edges, but also those over the whole energy range. This can be better visualized in k-space (see figure 6 in section 4). In order to check the reproducibility of the spectra, both EXAFS and MEXAFS data were collected on several Fe films for identical thickness ranges.

The oscillations in the extended energy region of both the EXAFS and the MEXAFS of the $L_{3,2}$ edge are related to a combination of the two edges, offset by the energy separation of the L_3 and L_2 edges. In k-space, the modulations in the EXAFS/MEXAFS signals can be expressed as

$$\chi(k) = \chi_{L3}(k) + \alpha\chi_{L3}(k + \Delta k) \tag{6}$$

with $\chi_{L2} \equiv \alpha\chi_{L3}$, where $\alpha = 1/2$ for the EXAFS and $\alpha = -1$ for the MEXAFS. That is to say, both spectra $\chi(k)$ and $\chi_M(k)$ contain the same basic information (near-neighbour distances, $A(k)$ etc), and the total experimental spectrum is just a superposition of these with a few fitting parameters. Note that the above-mentioned values of α are a good approximation for the 3d elements. The value of Δk steadily decreases as a function of k. For very large and very small spin–orbit splittings, α cannot be simply treated as a constant. Therefore, care has to be taken when analysing other systems.

Before starting to analyse the experimental data, we checked whether the superposition of the two edges hinders the analysis. This was done using *ab initio* curved-wave calculations, such as may be achieved with the FEFF7s code [21]. From this code it is possible to generate a simulation for L_3 and L_2 edges together and separately. We

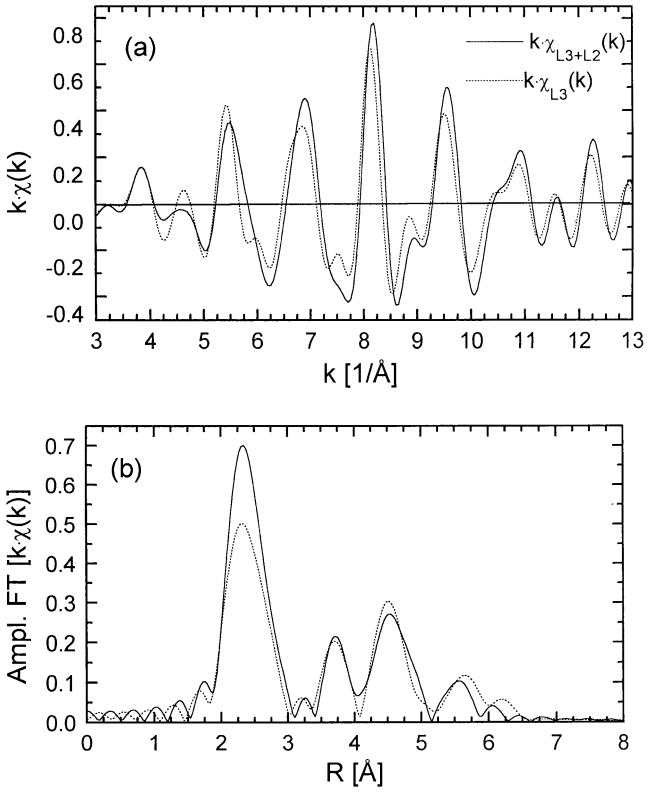

Figure 2. (a) The EXAFS signal $k\chi(k)$ simulated using the FEFF7s code for a bcc cluster, for the L_3 edge alone (dotted line) and the two edges together (solid line) and (b) their corresponding Fourier transforms. The superposition of the two edges causes an additional phase shift. The various peaks in the Fourier transforms merely show changes in their intensities.

have performed a FEFF simulation on a cluster of 369 Fe atoms having a bcc structure (the structural analysis is described in section 3). The simulated EXAFS signal $k\chi(k)$ for the two edges taken together (L_{3+2}) and the L_3 edge alone are shown in figure 2(a). Comparison of the two curves shows a slight difference in phase, which is due to the superposition of the two edges. In figure 2(b), corresponding Fourier transforms providing information regarding the neighbour distances and amplitude are shown. It is evident from the figure that the superposition of the two edges merely results in changes of intensity of the various features in the Fourier transforms and that their positions remain almost the same. Notice that the peaks of the Fourier transforms cannot simply be interpreted as distances of a particular shell. The real physical distance is an input parameter for the simulation. Similar simulations were also generated for the MEXAFS data. This was achieved with the FEFF7s code with a special card used to take care of left and right circular polarization [21]. The simulated MEXAFS signal $k\chi_M(k)$ and the corresponding Fourier transforms for the two cases are shown in figures 3(a) and 3(b). It is clear that for the MEXAFS also the superposition of the two edges merely results in changes of intensity of various features in the Fourier transforms. However, a comparison of figure 2(b) with figure 3(b) clearly shows that the effect of the superposition of the L_3 and L_2 edges is more dramatic in the magnetic case. We will come back to this in section 4. It should be pointed out here

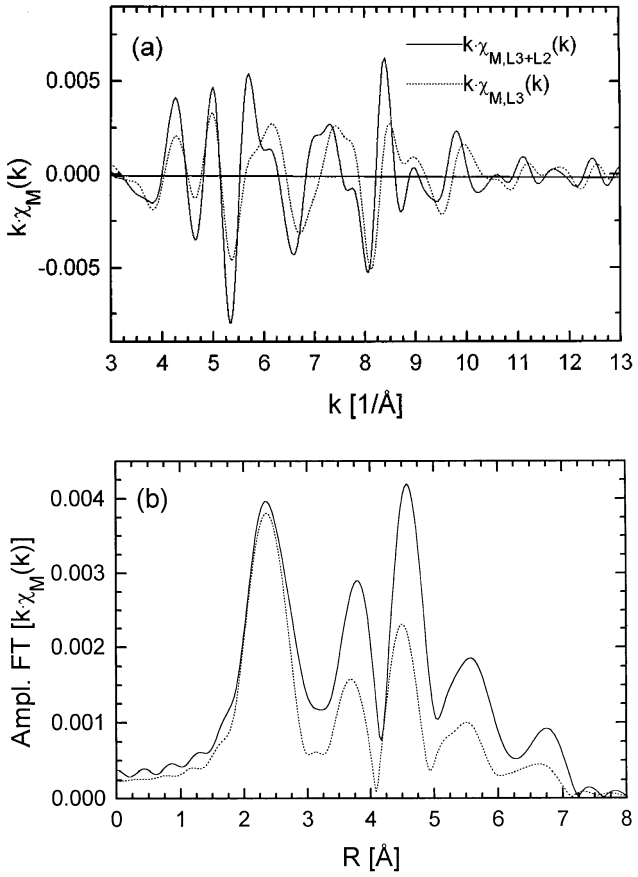

Figure 3. (a) The MEXAFS signal $k\chi_M(k)$ simulated using the FEFF7s code for a bcc cluster, for the L_3 edge alone (dotted line) and the two edges together (solid line) and (b) their corresponding Fourier transforms. The superposition of the two edges causes an additional phase shift and also contributes to an enhancement of various features in the Fourier transform between 3 and 6 Å.

that the intensities of the EXAFS and MEXAFS signals and their corresponding Fourier transforms shown in figures 2(a) and 2(b) and 3(a) and 3(b) cannot be compared directly to the simulations shown in sections 3 and 4. This is because in the present section our aim was merely to check the effect of superposition of the two edges, and therefore no damping parameters (which will be included in the theoretical input when we make a comparison with the experimental data) such as Debye–Waller factor were introduced.

3. EXAFS: structural and dynamical analysis

Figures 4(a) and 4(b) show the measured EXAFS signals $k\chi(k)$ and the corresponding Fourier transforms at two different temperatures at grazing x-ray incidence. First we will discuss the structure of the Fe films under study, i.e. the meaning of all of the features in the experimental Fourier transform for the data recorded at 75 K. In figure 5(a), the Fourier transform of the experimental spectrum recorded at 75 K for grazing incidence is shown along with a theoretical simulation performed using the FEFF7s code taking into

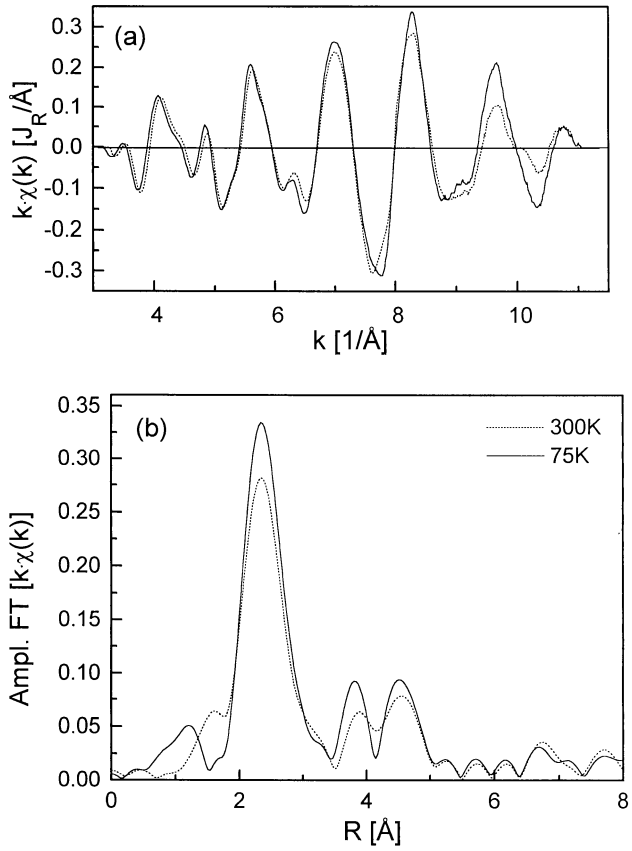

Figure 4. (a) The normalized EXAFS signal $k\chi(k)$ and (b) the corresponding Fourier transforms of Fe film 30 ML thick on Cu(001) measured at grazing x-ray incidence at 300 K (dotted line) and 75 K (solid line). A clear damping can be seen due to the excellent statistics and low noise level.

consideration both single-scattering (SS) and multiple-scattering (MS) paths. As can be seen from the figure, the simulation with a bcc unit cell (shown in the inset) taken as an input fits better to the experimental data than the one with a fcc unit cell. This clearly shows that the Fe film under study has predominantly a bcc structure. This is in accordance with other studies [19]. All of the main features observed in the Fourier transform could be reproduced in the theoretical simulations. The main peak is a superposition of two peaks, A and B. The nearest-neighbour peak A at 2.49 Å is ascribed to the single-scattering (SS) path between atoms 1 and 2 (see the inset in figure 5). Peaks B and C at 2.87 and 4.06 Å are due to the SS paths between atoms $1 \leftrightarrow 3$ and $1 \leftrightarrow 4$ respectively. The features D and E at 4.76 and 4.97 Å are ascribed to the SS and MS paths $1 \leftrightarrow 5$ and $1 \rightarrow 3 \rightarrow 4 \rightarrow 1$. In figure 5(b), we show theoretical simulations generated by taking into account just the SS paths (dotted line) as well as SS + MS paths (dashed line) for a bcc cluster and compare them with experimental Fourier transforms. It is clear that the majority of the features can be reproduced by SS simulation with a small contribution from MS.

Now, for the dynamical analysis, we turn to the spectra recorded at two different temperatures (figures 4(a) and 4(b)). Because of the excellent statistics, for the EXAFS

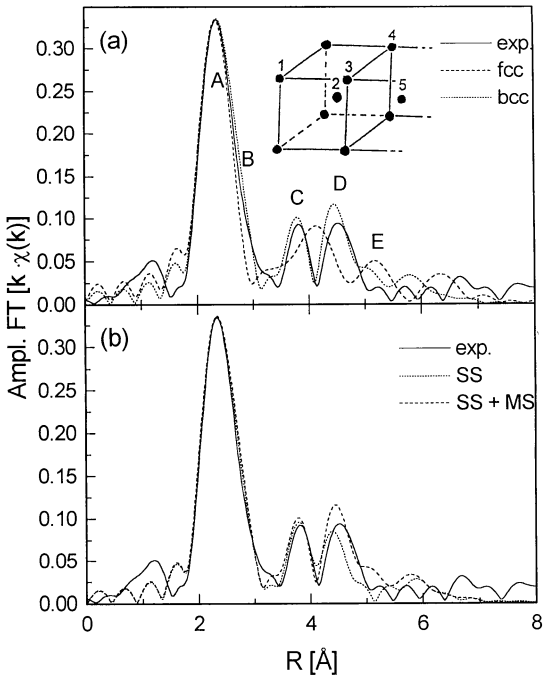

Figure 5. (a) Experimental and simulated Fourier transforms of the data recorded at grazing x-ray incidence at 75 K. It is clear that the simulation with a bcc cluster (the unit cell is shown in the inset) fits better to the experimental data than that with a fcc cluster. All of the features observed in the Fourier transform and the atoms in the unit cell are labelled, in order to show how they are ascribed to different scattering paths (see the text). The lower panel (b) shows Fourier transforms that were simulated taking into account both multiple- and single-scattering paths (dashed line) and just single-scattering paths (dotted line) along with the experimental data. It is clear that the majority of the contribution comes from the single-scattering paths. Note that the scale of the y-axis is not the same as that of figure 2 (see the text).

a damping can be seen that is outside the experimental error. To make it clearer, the static ($\sigma^2_{\rm stat}$) and dynamic ($\sigma^2_{\rm dyn}$) contributions to the Debye–Waller factor were calculated for the nearest-neighbour Fe–Fe coordinations. This was done in the following way. The amplitude of the nearest-neighbour peak (labelled as A in figure 5(a)) in the experimental Fourier transform was reproduced quantitatively in the simulated Fourier transform using the FEFF7s code [21]. This can be achieved by introducing a finite Debye–Waller factor ($\sigma^2_{\rm total}$) which includes both the static ($\sigma^2_{\rm stat}$) and the dynamic ($\sigma^2_{\rm dyn}$) contributions. The difference between the values of $\sigma^2_{\rm total}$ (experimental error $\approx$7%) obtained for the spectra measured at 300 K and 75 K yields $\Delta\sigma^2_{\rm dyn}$. For the present system, $\Delta\sigma^2_{\rm dyn}$ came out as 1.48×10^{-3} Å^2. Thereafter, iteratively an appropriate value of θ_D is obtained which fits well with $\Delta\sigma^2_{\rm dyn}$. In the present case θ_D was determined to be 560 K ($\pm$30%). Knowing this, one can now determine the static contribution to the Debye–Waller factor, which equals 3.0×10^{-3} Å^2. For bulk Fe, θ_D is estimated to be around 470 K from calorimetric measurements [22]. It was found [3] that θ_D determined by means of the EXAFS may be higher than the actual θ_D (determined by calorimetric measurements) if the phonon spectrum departs greatly from the Debye model. This is the case for bulk Fe. Nevertheless, the EXAFS θ_D which is calculated under the assumptions of the correlated Debye model is a useful parameter for

describing the temperature-dependent damping.

It is known that due to structural anisotropy and thermal disorder both the static and the dynamic contributions to the Debye–Waller factor can be anisotropic. This has been conclusively demonstrated for metals (e.g. in [23]) and low-Z adsorbates on metals (e.g. in [3, 4]). Such a complete dynamical analysis needs spectra for normal x-ray incidence, which is beyond the scope of the present work.

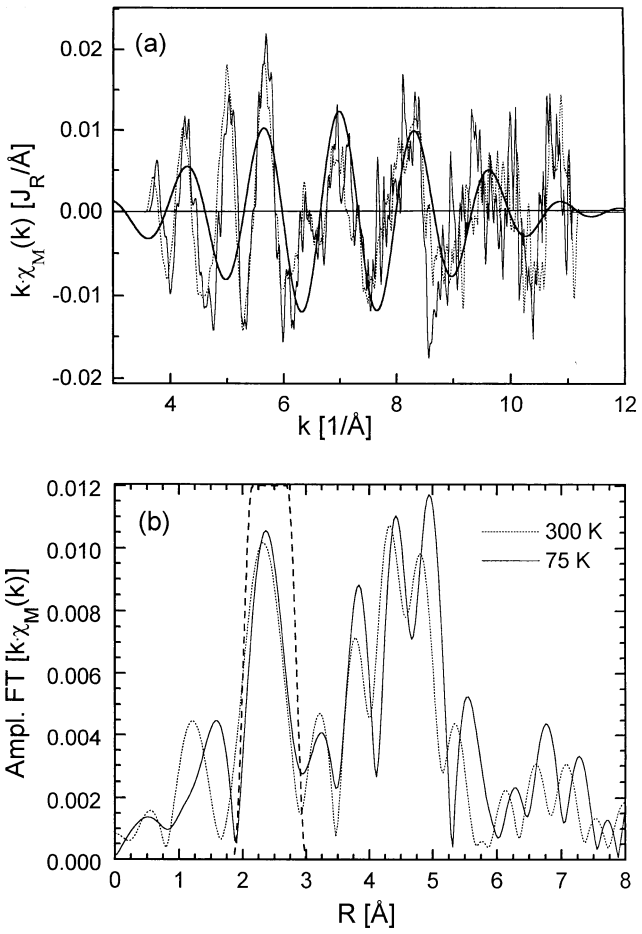

Figure 6. (a) The normalized MEXAFS signal $k\chi_M(k)$ and (b) the corresponding Fourier transforms of 30 ML Fe film on Cu(001) measured at grazing x-ray incidence at 300 K (dotted line) and 75 K (solid line). The backtransform of the nearest-neighbour peak is also shown in the upper panel (the thick solid line). The window function for this backtransform is shown as a dashed line. The high-frequency oscillations shown in the upper panel give rise to enhanced features between 3 and 6 Å.

4. MEXAFS analysis: experiment versus magnetic multiple-scattering calculations

Figures 6(a) and 6(b) show the measured MEXAFS signals $k\chi_M(k)$ and the corresponding Fourier transforms at two different temperatures at grazing x-ray incidence. As is evident from figures 6(a) and 4(a), the relative magnetic contribution (MEXAFS) is about 3%

compared to the amplitude of the spin-averaged EXAFS oscillations. In accordance with the results of previous studies (e.g. [5]), the amplitude of the χ_M-oscillations is largest at the low k-values, while the EXAFS amplitudes show their maximum in the intermediate k-range. However, it should be pointed out that, apart from the higher-frequency components resulting from the increased contribution of the longer scattering path lengths, the present χ_M-profiles clearly show slow oscillations at intermediate and high k-values. This indicates the high quality of the present data. As we have pointed out in section 1, 'fast' oscillations have already been discussed in the literature; in view of this, we show, in figure 6(a), the Fourier backtransform (the bold solid line) of the nearest-neighbour peak. It is clear that the backtransformed main peak describes the experimental data between 6 and 11 Å^{-1} quite well, implying that the oscillations in this region follow the main frequency with some superposition from the higher frequencies. These higher frequencies are not only due to the backscattering from more distant shells of neighbours, but also to multiple-scattering effects. The 'fast' oscillations between 4 and 6 Å^{-1} are dominated by peaks with enhanced intensities between 3.5 and 5 Å in the Fourier transform. The two regions can be analysed together or independently, according to requirements.

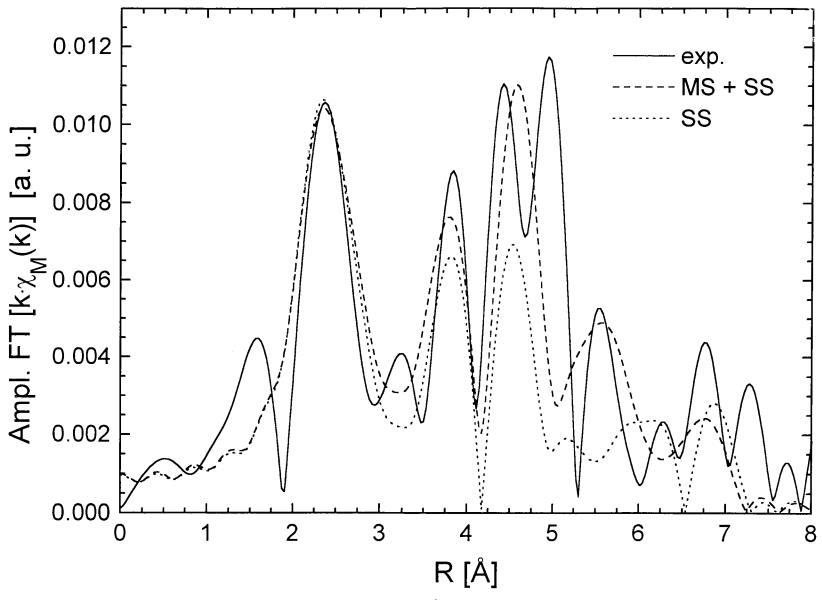

Figure 7. Simulated Fourier transforms (taking $\sigma^2 = 0$) taking into account both multiple- and single-scattering paths (dashed line) and just single-scattering paths (dotted line) for a bcc cluster, along with the experimental (solid line) MEXAFS data recorded at grazing x-ray incidence at 75 K. It is clear that the single-scattering paths contribute significantly. The nearest-neighbour peak obtained in the simulations is scaled to that obtained from experiment.

One purpose of the present study was to see whether theory and experiment agree for the L-edge MEXAFS of 3d elements. A theoretical simulation with a bcc unit cell using FEFF7s was performed and is shown together with the Fourier transform of the experimental spectrum recorded at 75 K in figure 7. The spectrum (dashed line) representing the simulation generated by taking into account both single- and multiple-scattering paths is in qualitative agreement with the experimental Fourier transform. Also, a simulation (dotted curve) taking into account only the SS paths is shown. The peak at 2.49 Å was scaled by a

factor of 9.5, the experimental results being larger than those from theory. The simulation establishes that the peak at around 3.8 Å contains a significant contribution from a SS path. The simulated peak at around 4.5 Å is strongly influenced by MS contributions; however, the experimental Fourier transform shows a splitting of the peak. Finally, the peak at 5.5 Å is totally due to MS. As discussed in the previous section, various features between 3.5 and 5 Å in the Fourier transform showing enhancement in intensity are due to the 'fast' oscillations shown in figure 6(a). Therefore, the present theoretical analysis suggests that these high-frequency contributions do contain appreciable contributions from SS and MS path lengths. This in turn implies that the magnetic character of both single- and multiple-scattering path lengths increases. One may argue that this increase is due to the overlapping of Fe L_3 and L_2 edges. However, if one compares the simulated Fourier transforms for the EXAFS and MEXAFS taking into consideration just the L_3 edge (see figures 2(b) and 3(b)), it is quite apparent that these contributions are different for the EXAFS and MEXAFS. Nevertheless, a contribution to these high-frequency components due to the overlap of L_3 and L_2 edges cannot be ruled out. Also, if one compares figure 4(a) with figure 6(a), it is clear that the EXAFS and MEXAFS oscillations are not in phase. However, the phase difference is not $\pi/2$ as expected theoretically, since for the $L_{3,2}$ edges the EXAFS and the MEXAFS should be derivatives of each other. This is due to the superposition of the two edges, which causes additional phase shifts.

In the present analysis, we have focused on the features between 2.2 and 5.5 Å in the Fourier transform shown in figures 6(b) and 7. However, spin-dependent scattering above 6–7 Å can be seen clearly. This may be due to scattering from more distant shells or multiple-scattering effects. We also see a peak at around half of the nearest-neighbour distance ($R = 1.1$–1.2 Å) which may originate from the so-called spin-dependent atomic EXAFS arising from scattering within the embedded atom (interstitial spin/charge density). This has been discussed in [8] for metals (Gd, Tb) and alloys ($HoFe_2$) for magnetic EXAFS. For normal EXAFS, a similar low-frequency structure was unambiguously identified, and this has been discussed in detail in [24]. This peak does not show up in the present simulation (see figure 7) because the theoretical input does not take into account scattering from the interstitial spin/charge densities. Both effects will be discussed in a future publication.

Now we discuss briefly the temperature dependence of the MEXAFS spectra. It is clear from figure 6 that the MEXAFS oscillations do not show an appreciable temperature dependence. For the MEXAFS the signal is smaller by 1/34, and consequently the statistics is worse and therefore a clear damping cannot be observed. However, this remains unexpected, because the spin fluctuation should be rescaled to the Curie temperature, which in this case should be approximately equal to 1050 K, and therefore even the 300 K value corresponds to a reduced temperature of $T/T_C \approx 0$.

5. Conclusions

The present study shows that a meaningful analysis of MEXAFS data can be carried out at the L edges of transition metals. The present EXAFS and MEXAFS analysis of a well characterized 30 ML Fe film on Cu(001) enables us to compare both structural and dynamical aspects of the two cases. The present investigation demonstrates the usefulness of combining *ab initio* calculations with experiments for the MEXAFS. With the help of theoretical calculations one can qualitatively identify various peaks (frequencies) up to $R = 6$ Å. All of the contributions to nearest shells from single- and multiple-scattering path lengths can be modelled separately. Also, temperature-dependent damping was found to occur to a lesser extent for MEXAFS than for normal EXAFS. For the present system,

even for normal EXAFS it was not very pronounced between 75 K and 300 K. Therefore, spectra recorded at higher temperatures would be useful. The reasonably large ratio ($\sim 1/34$) between the normal and magnetic EXAFS amplitudes will be of importance for future applications in studying the spin dynamics of 3d magnets in detail. Similar analysis has been successfully applied to Co films on Cu(001) [25].

Acknowledgments

We thank F May for his help in the initial stages of the experiment. A Ney is acknowledged for his help during the measurements. H Ebert and D Ahlers are acknowledged for fruitful discussions. We are grateful to Y Idzerda for providing us with data prior to publication. This work was supported by DFG SFB 290 and BMBF (05621 KEA5) grants. One of us (PS) is grateful to the Alexander von Humboldt (AvH) foundation for financial support.

References

[1] See, for example,
Teo B K 1986 *EXAFS: Basic Principles and Data Analysis* (Berlin: Springer)
Arvanitis D and Baberschke K 1995 *J. Electron. Spectrosc. Relat. Phenom.* **75** 149 and references therein

[2] See, for example,
Bunker G 1983 *Nucl. Instrum. Methods* **207** 437
and for a review, see
Crozier E, Rehr J and Ingals R 1988 *X-Ray Absorption: Principals, Applications, Techniques of EXAFS, SEXAFS and XANES (Wiley Series on Chemical Analysis 92)* ed D C Konigsberger and R Prins (New York: Wiley)

[3] Tröger L, Yokoyama T, Arvanitis D, Lederer T, Tischer M and Baberschke K 1994 *Phys. Rev.* B **49** 888

[4] Lederer T, Arvanitis D, Comelli G, Tröger L and Baberschke K 1993 *Phys. Rev.* B **48** 15 390

[5] Schütz G, Wagner W, Wilhelm W, Kienle P, Zeller R, Frahm R and Materlik G 1987 *Phys. Rev. Lett.* **58** 737

[6] Schütz G, Frahm R, Mautner P, Wienke R, Wagner W, Wilhelm W and Kienle P 1989 *Phys. Rev. Lett.* **62** 2620

[7] Schütz G, Knülle M and Ebert H 1993 *Phys. Scr.* T **49** 302

[8] Schütz G and Ahlers D 1995 *Herrsching Proceedings (Springer Lecture Notes in Physics 466)* ed H Ebert and G Schütz (Berlin: Springer) p 229

[9] Chakarian V, Idzerda Y U, Kemner K M, Park J-H, Meigs G and Chen C T 1996 *J. Appl. Phys.* **79** 6493

[10] Idzerda Y U, Chakarian V and Freeland J W 1997 *Synchrotron Radiat. News* **10** 6

[11] Isnard O, Miraglia S, Fruchart D, Giorgetti C, Pizzini S, Dartyge E, Krill G and Kappler J P 1994 *Phys. Rev.* B **49** 15 692

[12] Kobayashi K, Maruyama H, Maeda H, Iwazumi T, Kawata H and Yamazaki H 1995 *Physica* B **208+209** 779

[13] Dartyge E, Baudelet F, Brouder C, Fontaine A, Giorgetti C, Kappler J P, Krill G, Lopez M F and Pizzini S 1995 *Physica* B **208+209** 751

[14] Schütz G, Fischer P, Attenkofer K, Knülle M, Ahlers D, Stähler S, Detlefs C, Ebert H and de Groot F 1994 *J. Appl. Phys.* **76** 6453

[15] Knülle M, Ahlers D and Schütz G 1995 *Solid State Commun.* **94** 267

[16] Brouder C and Hikam M 1991 *Phys. Rev.* B **43** 3809

[17] Schütz G, Fischer P, Goering E, Attenkofer K, Ahlers D and Rößl W 1997 *Synchrotron Radiat. News* **4** 13

[18] Boyce J B and Baberschke K 1981 *Solid State Commun.* **39** 781

[19] Li D, Freitag M, Pearson J, Qiu Z Q and Bader S D 1994 *Phys. Rev. Lett.* **72** 3112
Müller S, Bayer P, Reischl C, Heinz K, Feldmann B, Zillgen H and Wuttig M 1995 *Phys. Rev. Lett.* **74** 765

[20] Hunter Dunn J, Arvanitis D, Mårtensson N, Tischer M, May F, Russo M and Baberschke K 1995 *J. Phys. C: Solid State Phys.* **7** 1111

[21] Ankudinov A and Rehr J J 1996 *Phys. Rev.* B **52** 10 214
Ankudinov A and Rehr J J 1997 *Phys. Rev.* B **56** R1712

[22] *Zahlenwerte und Funktionen aus Naturwissenschaft und Technik; Landolt–Börnstein New Series* 1981 Group III, vol 13a (Berlin: Springer) p 53
[23] Chandesris D 1986 *J. Physique Coll.* **47** C8 479
[24] Wende H, Srivastava P, Chauvistré R, May F, Baberschke K, Arvanitis D and Rehr J J 1997 *J. Phys. C: Solid State Phys.* **9** L427
[25] Lemke L 1997 *Diploma Thesis* FU Berlin